Quaternary ammonium silane, calcium and phosphorus-loaded PLGA submicron particles against *Enterococcus faecalis* infection of teeth: An *in vitro* and *in vivo* study

Wei Fan[a,1], Yanyun Li[a,1], Qing Sun[a], Franklin R. Tay[b], Bing Fan[a,*]

[a] *The State Key Laboratory Breeding Base of Basic Science of Stomatology (Hubei-MOST) and Key Laboratory of Oral Biomedicine Ministry of Education, School and Hospital of Stomatology, Wuhan University, Wuhan, People's Republic of China*
[b] *Department of Endodontics, The Dental College of Georgia, Augusta University, Augusta, GA, USA*

ARTICLE INFO

ABSTRACT

Refractory root canal infection of human teeth is the primary cause of dental treatment failure. *Enterococcus faecalis* is the major cause of refractory root canal infection. In the present study, poly(D,L-lactic-*co*-glycolide) (PLGA) submicron particles were used as carriers to deliver an antimicrobial quaternary ammonium silane (code-named K21) as well as calcium and phosphorus elements. The release profiles, antibacterial ability against *E. faecalis*, extent of infiltration into dentinal tubules, biocompatibility and *in vitro* mineralization potential of the particles were investigated. In addition, the antimicrobial effects of the particles against *E. faecalis* infection were evaluated *in vivo* in the teeth of beagle dogs. The encapsulated components were released from the PLGA particles in a sustained-release manner. The particles also displayed good biocompatibility, *in vitro* mineralization ability and antibacterial activity against *E. faecalis*. The particles could be driven into dentinal tubules of dentin slices by ultrasonic activation and inhibited *E. faecalis* colonization. In the root canals of beagle dogs, PLGA submicron particles loaded with K21, calcium and phosphorus demonstrated strong preventive effects against *E. faecalis* infection. The system may be developed into a new intracanal disinfectant for root canal treatment.

1. Introduction

Enterococcus faecalis, a gram-positive facultative anaerobe, is involved in many severe infections of the human body. In dentistry, *E. faecalis* is the predominant bacteria responsible for refractory root canal infections and treatment failures [1]. *Enterococcus faecalis* is capable of colonizing the root canals of teeth when inoculated alone in pure culture [2]. This bacterium not only attaches to canal wall dentin, but also penetrates deeply into the dentinal tubules to a depth of up to 1500 μm [3]. Other virulence factors of *E. faecalis* include the ability to form biofilm, the ability to express survival genes and modulate host immune system [4,5]. *E. faecalis* could also form mixed plaque and biofilm with other microorganisms, increasing resistance to bactericide [6]. Besides, *E. faecalis* is intrinsically resistant to cephalosporins and aminoglycosides and may acquire resistance to vancomycin [7–9]. Conventional root canal antimicrobial medications such as silver ions, calcium hydroxide and sodium hypochlorite, show limited antibacterial effects

against *E. faecalis* either because of the resistance of *E. faecalis* against these medications, or inadequate infiltration of the medicaments into the dentinal tubules [10–14]. Scholars are also trying to apply other treatment strategies against *E. faecalis*, such as with bacteriophages and phage cocktails [15,16].

Quaternary ammonium compounds are surfactants and possess potent broad-spectrum bactericidal effects [17]. These compounds penetrate bacterial cell walls and interact with the phospholipid bilayer of membranes, resulting in the leakage of intracellular components [18]. In dentistry, quaternary ammonium compounds have been incorporated into resin adhesives, dental pulp capping agents and implants for antimicrobial modifications [19–21]. 1-octadecanaminium, N,N′-[[3,3-bis[[[3-(dimethyloctadecylammonio)propyl] dihydroxysilyl]oxy]-1,1,5,5-tetrahydroxy-1,5-trisiloxanediyl]di-3,1-propanediyl]bis[*N,N*-dimethyl-],chloride 1:4 ($C_{92}H_{204}Cl_4N_4O_{12}Si_5$, CAS number 1566577-36-3; code-named K21, Fig. 1) is an antimicrobial quaternary ammonium silane synthesized *via* sol-gel reaction of tetraethoxysilane

---

* Corresponding author at: The State Key Laboratory Breeding Base of Basic Science of Stomatology (Hubei-MOST) and Key Laboratory of Oral Biomedicine Ministry of Education, School and Hospital of Stomatology, Wuhan University, 237 Luoyu Road, Wuhan 430079, People's Republic of China.
E-mail address: bingfan@whu.edu.cn (B. Fan).
[1] Co-first authors with equal contributions.
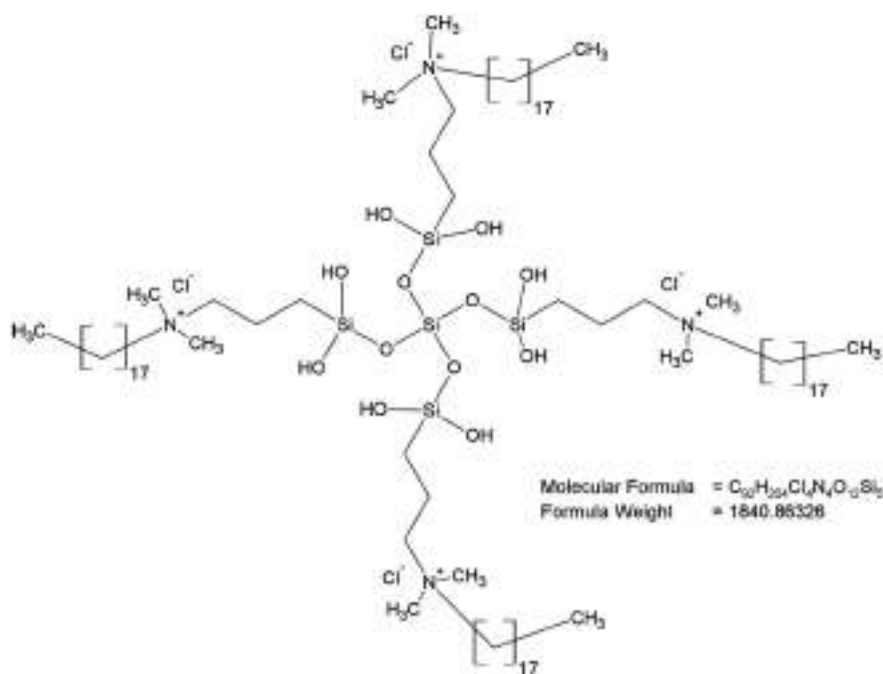
Fig. 1. Idealized chemical structure of the quaternary ammonium silane employed in the present study.

(TEOS) and 3-(triethoxysilyl)-propyldimethyloctadecyl ammonium chloride. Inclusion of TEOS as an anchoring unit provides a three-dimensional organically-modified silicate network [22]. As a cavity cleanser for disinfecting decayed teeth prior to filling, K21 inhibits the growth of *Streptococcus mutans* and *Actinomyces naeslundii* effectively without adversely affecting dentin bond strength [23]. In addition, K21 also possesses anti-viral effects against Herpes simplex type 1, Human herpesvirus (HHV)-6A and HHV-7 [24].

Calcium and phosphorus are components of human hard tissues including bones and teeth, and are closely related to the osteogenic process [25,26]. Biomaterials containing calcium and phosphorus are frequently used for the restoration of bone defects, improvement of implant osteoconductivity and remineralization of teeth [27–29]. The Ca/P ratio is an important parameter to be considered in pro-osteogenic biomaterials design [30]. Addition of silicate to releasable calcium phosphate formulations has been reported to significantly enhance the osteogenic effect of biomaterials *in vitro* and *in vivo* [31,32].

Poly(D,L-lactic-*co*-glycolide) (PLGA) is a biodegradable polymer synthesized by ring-opening polymerization or polycondensation reaction of lactic and glycolic acids [33,34]. The biocompatibility of PLGA has been well proven [35–37]. Materials prepared with PLGA have been used as drug delivery vehicles and tissue engineering scaffolds [38–40]. Submicron and nanoscopical particles of PLGA demonstrate better infiltration capability and appear to be the preferred candidate as a root canal disinfectant carrier [41–43].

Based on the aforementioned considerations, submicron PLGA particles loaded with quaternary ammonium silane, calcium and phosphorus were synthesized. The release profiles, antibacterial ability against *E. faecalis*, extent of infiltration into dentinal tubules, biocompatibility and *in vitro* mineralization potential of the particles were investigated. In addition, beagle dogs were used as a tooth infection animal model to evaluate the effects of PLGA submicron particles against *E. faecalis* infection *in vivo*. Accordingly, the hypothesis tested in the present study was that K21-, calcium- and phosphorus-loaded PLGA submicron particles possess antimicrobial and mineralization activities and inhibit *E. faecalis* root canal infection *in vitro* and *in vivo*.

2. Materials and methods

2.1. Synthesis

Submicron PLGA particles containing K21, calcium and phosphorus (P-CaPK) were synthesized according to a modified emulsion-solvent evaporation method [42]. Briefly, 200 mg PLGA with a 50:50 lactic acid to glycolic acid ratio (Mw 38,000–54,000) (MilliporeSigma, St. Louis, MO, USA) was dissolved in 10 mL dichloromethane (Sinopharm Chemical Reagent Co. Ltd., Shanghai, China) at room temperature. This was followed by slow addition of 0.313 mL of 0.5 M calcium nitrate tetrahydrate (Sinopharm) solution, 0.313 mL of 0.3 M sodium dihydrogen phosphate dihydrate (Sinopharm) solution and 1.25 mL of 20% (w/v) K21 (FiteBac, Marietta, GA, USA) alcoholic solution. After mixing, the blend was poured into 20 mL of 1.5% (w/v) poly(vinly alcohol) (Mw 146,000–186,000; MilliporeSigma) aqueous solution. The mixture was emulsified using a homogenizer for 10 min at 11000 rpm. Eighty milliliter of double-distilled water (dd H_2O) was then added and the solution was stirred at ambient temperature to evaporate the dichloromethane. The submicron particles were collected using a centrifuge and washed three times with dd H_2O. The powder was frozen at −80 °C and lyophilized (LyoQuest −85Plus, Telstar, Terrassa, Spain).

For comparison, pure PLGA submicron particles, PLGA submicron particles containing calcium nitrate tetrahydrate and sodium dihydrogen phosphate dihydrate, PLGA submicron particles containing only K21 were also prepared according to the aforementioned procedures. These particles were referred to as P, P-CaP and P−K respectively. Table 1 listed related abbreviations and their meanings.

Table 1
Related abbreviations and meanings.

Abbreviations	Full name
P	PLGA submicron particles
P-K	PLGA submicron particles containing K21
P-CaP	PLGA submicron particles containing calcium and phosphorus
P-CaPK	PLGA submicron particles containing K21, calcium and phosphorus
CHX	Chlorhexidine

2.2. Physical characterization

Field–emission scanning electron microscopy (FE-SEM; Sigma, Carl Zeiss Microscopy GmbH, Jena, Germany) was used to examine the morphology of P, P-CaP, P−K and P-CaPK. The elemental composition of the submicron particles was analyzed by energy dispersive spectrometry (EDS; Quanta 200, Thermo Fisher Scientific, Waltham, MA, USA). Particle size distribution and zeta potential were measured by dynamic light scattering (Zetasizer Nano ZSP, Malvern Instruments Ltd., Malvern, UK). Loading of K21 within PLGA was confirmed by Fourier transformed infrared spectroscopy (FTIR; Nicolet5700, Thermo Fisher Scientific).

2.3. Drug encapsulation efficiency (EE) and loading content (LC)

The EE and LC of calcium and phosphorus were determined by dissolving a certain amount of particles in dichloromethane. Tris–HCl (1 M, pH 7.4) was subsequently used to extract calcium and phosphorus. The amounts of calcium and phosphorus were measured by inductively coupled plasma-atomic emission spectrometry (ICP-AES; IRIS Intrepid II XSP, Thermo Fisher Scientific). For the EE and LC of K21, the absorbance of dichloromethane was measured at 228 nm using a spectrometer (UV-2401PC, Shimadzu Corp. Kyoto, Japan). Determination of EE was performed according to the formula: drug amount encapsulated in particles/initial drug amount. Determination of LC was performed according to the formula: drug amount encapsulated in particles/total particle amount. All tests were performed in triplicate.

2.4. pH and release profile

The change in pH value over time was determined by immersing 100 mg of P, P-CaP, P−K or P-CaPK in 20 mL of dd H_2O at 37 °C. The pH value of respective solution was measured at 1, 3, 6, 9, 15, 21, 27 days using a pH meter (Sarto-rius AG, Goettingen, Germany).

The calcium and phosphorus release profiles were determined by soaking 20 mg of P-CaP or P-CaPK in 10 mL of Tris-HCl at 37 °C. Five milliliter of Tris-HCl was retrieved after 1, 3, 6, 9, 15, 21 and 27 days for ICP-AES. Solution retrieval was simultaneously accompanied by replacement of 5 mL of fresh Tris-HCl in the respective solution. The cumulative amount of released elements was calculated.

The amount of released K21 was estimated by placing 20 mg of P−K or P-CaPK in 10 mL of dd H_2O at 37 °C. At the same time interval, the absorbance of 1 mL of the supernatant was evaluated spectrophotometrically at 218 nm. All experiments were conducted in triplicate.

2.5. Antibacterial activity against planktonic E. faecalis

The colony-forming unit (CFU) counting method was used to evaluate the antimicrobial activities of P, P-CaP, P−K and P-CaPK. *Enterococcus faecalis* (ATCC 29212, ATCC, Manassas, VA, USA) was cultured and adjusted to a concentration of 1×10^4 CFUs/mL in brain heart infusion (BHI) medium. Then, 1 mL of bacteria suspension was incubated with 1, 2 and 5 mg of submicron particles respectively for 24 h at 4 °C. The positive control consisted of 2% chlorhexidine digluconate (CHX) solution and the negative control consisted of bacteria suspension without particle addition. Ten microliter of the suspension was inoculated on a BHI agar plate and cultured anaerobically at 37 °C for 24 h. The CFUs of *E. faecalis* formed on each plate were counted. For each group, the experiment was conducted in sextuplicate.

2.6. Cytotoxicity evaluation

Cytotoxicity of P, P-CaP, P−K and P-CaPK was evaluated using the cell counting kit-8 (CCK-8; Dojindo Laboratories, Kumamoto, Japan) on MC3T3-E1 cells (CRL-2594, ATCC). Ten milligram of P, P-CaP, P−K or

P-CaPK was soaked in 1 mL of α-MEM (Thermo Fisher Scientific) at 37 °C for 24 h. The supernatant was collected with centrifuge and sterilized using a 0.22 μm filter unit (Merck KGaA, Darmstadt, Germany). This was followed by supplementation of 10% fetal calf serum (FCS; Thermo Fisher Scientific). Dilutions of 2, 4 and 10 mg/mL were prepared.

MC3T3-E1 cells were cultured and adjusted to 8.0×10^4 cells/mL. One hundred microliter of cell suspension was seeded in each well of a 96-well plate and incubated at 37 °C with 5% CO_2. This was replaced with 100 μL fresh α-MEM with 10% fetal calf serum and 1% penicillin/streptomycin (Thermo Fisher Scientific) after 24 h, followed by the addition of 100 μL extract of submicron particles. The wells containing only α-MEM and the wells containing cells without extracts were used as controls. Each group included six wells. After 2, 4 and 6 days, cells were washed 3 times with α-MEM. Then, 100 μL α-MEM and 10 μL CCK-8 were added to each well and incubated at 37 °C for 3 h. Absorbance was measured at 450 nm using a micro-plate reader (Power Wave XS2, BioTek Instruments, VT, USA).

2.7. Dentinal tubule infiltration and inhibition of E. faecalis

The teeth used for preparing dentin slices were collected under the approval of ethics committee of School and Hospital of Stomatology, Wuhan University. To investigate the infiltration capability of P−K and P-CaPK into dentinal tubules, dentin slices (4 mm × 4 mm × 1 mm thick) were prepared from extracted premolars and molars with a low-speed saw with water cooling. The slices were cleaned ultrasonically in dd H_2O, 5.25% NaOCl and 17% EDTA successively for 4 min each and finally in dd H_2O for one more min.

After disinfection by autoclaving, each dentin slice was immersed in 500 μL of 20 mg/mL particle suspension. Passive ultrasonic vibration was performed using an ultrasonic file to drive the particles into the dentinal tubules. The power of the ultrasonic device (P5, Satelec, Merignac, France) was set at scale 4. The ultrasonic file was located 1 mm away from the dentin slice, parallel to the dentin surface, and vibration was performed on each side for 60 s. The dentin slices were rinsed with dd H_2O and split into two halves with hammer and chisel to expose the longitudinal sections of the dentinal tubules. Infiltration of P−K and P-CaPK into the tubules was observed by FE-SEM.

The antimicrobial effect of P, P-CaP, P−K and P-CaPK on *E. faecalis*-infiltrated dentin was examined by infiltrating the dentin slices with particle suspensions, using ultrasonic vibration as previously described. Then, 1 mL suspension of *E. faecalis* (1×10^4 CFUs) was incubated with each dentin slice for bacterial colonization at 37 °C under anaerobic conditions for 7 days. Dentin slices treated ultrasonically with sterile dd H_2O were used as controls. The dentin slices were then immersed in 5 mL of fresh BHI solution after rinsing with 1 mL sterile phosphate buffer saline (PBS) for three times. The optical density (OD) values of 1 mL BHI solution were measured by a spectrometer at 600 nm after 2, 4, 6 and 8 h. Each group included 6 slices. In addition, FE-SEM was used to examine one additional slice from each group after bacteria incubation to identify colonized bacteria on the dentin surface.

2.8. In vitro mineralization

The teeth used for preparing dentin blocks were collected under the approval of ethics committee of School and Hospital of Stomatology, Wuhan University. The *in vitro* mineralization capability of the submicron particles was investigated by preparing dentin blocks from extracted premolars. Single-rooted premolars with closed apices were selected and dental crowns were removed using a low-speed saw with water cooling. The root canals in each tooth were instrumented to size F3 using ProTaper nickel titanium rotary instruments (Dentsply Sirona, Charlotte, NC, USA). Root blocks (1.5 mm thick) were subsequently prepared by sectioning the coronal part of each root perpendicular to its longitudinal axis. The root blocks were cleaned ultrasonically according
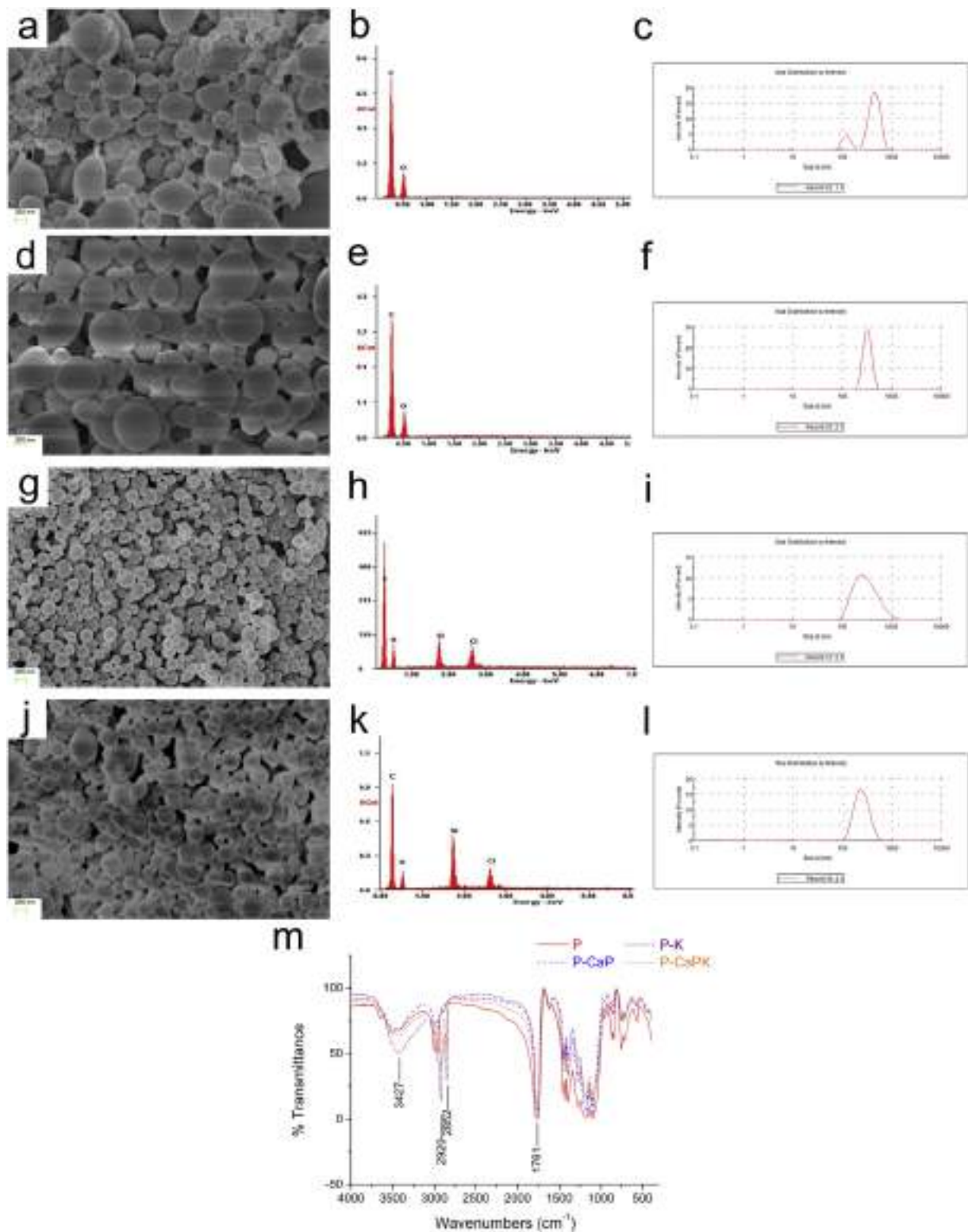
Fig. 2. Characterization of P, P-CaP, P−K and P-CaPK. a. SEM image of P; b. EDS analysis of P; c. size distribution graph of P; d. SEM image of P-CaP; e. EDS analysis of P-CaP; f. size distribution graph of P-CaP; g. SEM image of P-K; h. EDS analysis of P-K; i. size distribution graph of P-K; j. SEM image of P-CaPK; k. EDS analysis of P-CaPK; l. size distribution graph of P-CaPK; m. FTIR spectrum of P, P-CaP, P−K and P-CaPK.

to the method described in 2.7 and autoclaved.

Simulated body fluid (SBF) was prepared according to Kokubo and Takadama's formulation [44]. The P, P-CaP, P−K and P-CaPK particles were compacted into the root canals of the root blocks and immersed in SBF for 3 weeks at 37 °C. The retrieved root blocks were examined with FE-SEM and EDS to characterize the CaP precipitated on dentin.

2.9. Animal study

The animal experiment was approved by the ethics committee of School and Hospital of Stomatology, Wuhan University and the Institutional Review Board, Hubei Institute Co., Ltd. of Pharmaceutical Industry.

Table 2
Average diameter, zeta potential and quantitative EDS analysis of the element proportion in P, P-CaP, P—K and P-CaPK.

	Diameter (nm)	Zeta potential (mV)	C (wt%)	O (wt%)	Si (wt%)	Cl (wt%)
P	727.97 ± 71.52	−17.87 ± 2.38	73.92	26.08		
P-CaP	647.2 ± 75.70	−12.00 ± 0.71	74.26	25.74		
P-K	256.43 ± 10.75	35.67 ± 1.11	77.30	18.65	2.19	1.86
P-CaPK	256.37 ± 29.81	33.97 ± 1.62	78.86	15.29	4.13	1.72

Table 3
Encapsulation efficiency (EE) and loading content (LC) of K21, calcium and phosphorus.

	K21		Calcium		Phosphorus	
	EE (%)	LC (%)	EE (%)	LC (%)	EE (%)	LC (%)
P-CaP	–	–	19.06 ± 0.54	0.60 ± 0.02	13.52 ± 0.43	0.20 ± 0.01
P-K	28.25 ± 5.30	35.31 ± 6.63	–	–	–	–
P-CaPK	28.34 ± 4.17	35.42 ± 5.22	18.32 ± 0.54	0.57 ± 0.02	12.71 ± 0.49	0.19 ± 0.01
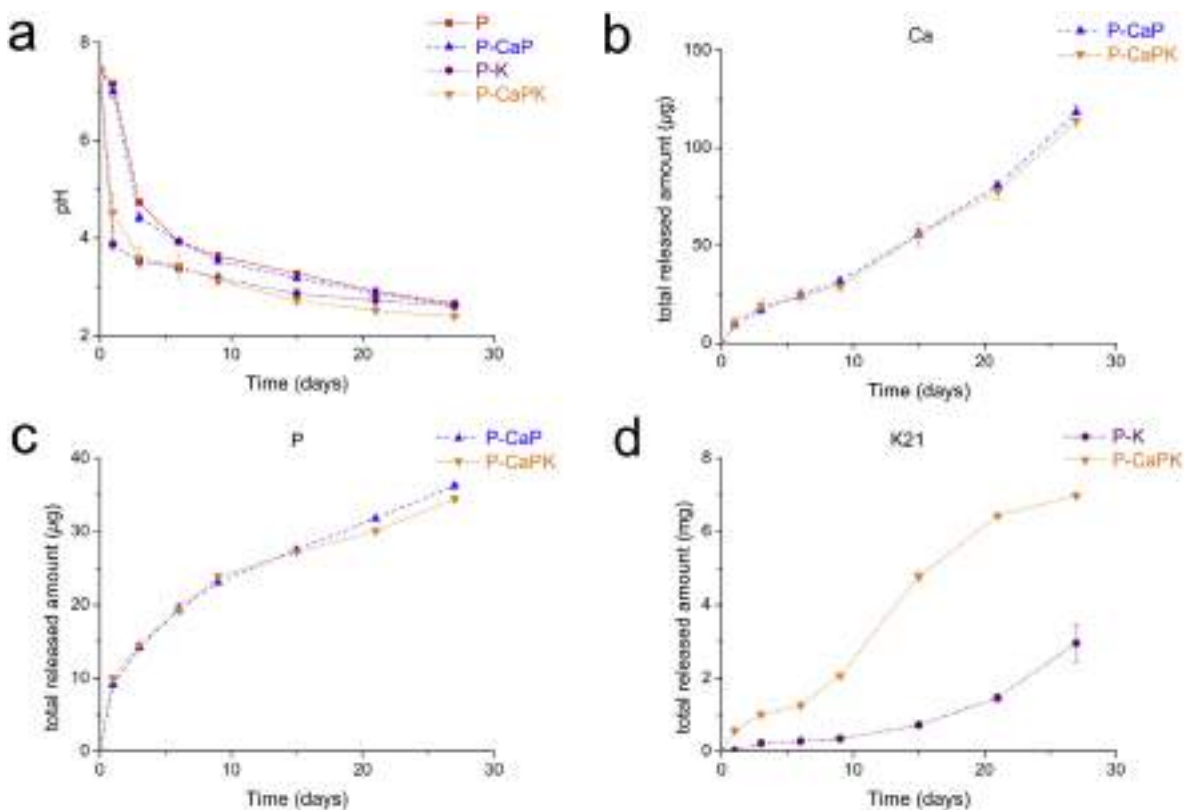
Fig. 3. pH measurement and release profiles of P, P-CaP, P—K and P-CaPK. a. pH measurement in dd H_2O; b. calcium release; c. phosphorus release; d. K21 release.

Five healthy female beagle dogs (12–18 months) were used to investigate the inhibitory effects of P-CaPK against *E. faecalis* tooth infection *in vivo*. The animals were anesthetized by intravenous injection of 3.5% pentobarbital sodium (Merck KGaA, Darmstadt, Germany; 1 mL/kg), supplemented by intraperitoneal injection of 0.25 mL/kg pentobarbital sodium when necessary. Preoperative periapical radiographs of the bilateral mandibular second and third premolars were taken using a paralleling technique. A rubber dam was placed after local anesthesia with Primacaine. After removal of pulpal tissues from each premolar, the working length was determined using an electronic apex locator (PROPEX II, Dentsply Sirona). All root canals were instrumented to size F3 with ProTaper nickel titanium rotary instruments. Irrigation was performed successively with 5 mL of 5.25% NaOCl, 17% EDTA and normal saline (NS). Calcium hydroxide paste (powder/water ratio: 200 mg/400 μL), 2% CHX solution, 20 mg/mL P-CaPK suspension or NS was randomly assigned as intracanal medicament to each tooth. After placement of the medicament, each root canal was ultrasonicated at scale 4 for 1 min. The access cavities were temporized with glass ionomer cement (Changshu Shangchi Dental Materials Co., Ltd., China). Meloxicam tablets (Yangtze River Pharmaceutical Co. Ltd., China) was administered orally twice a day in the first two days after surgery and a soft diet was provided.

General anesthesia was performed after one week with intramuscular injection of xylazine hydrochloride (3 mg/kg), followed by intravenous injection of 3.5% pentobarbital sodium (0.2 mL/kg). The glass ionomer cement was removed and the root canals were irrigated with NS. *Enterococcus faecalis* suspensions (10^8 CFUs/mL) were injected into the root canals. This was followed by sealing the access cavities with glass ionomer cement. Periapical radiographs were taken every two weeks to observe the progress of apical lesions.
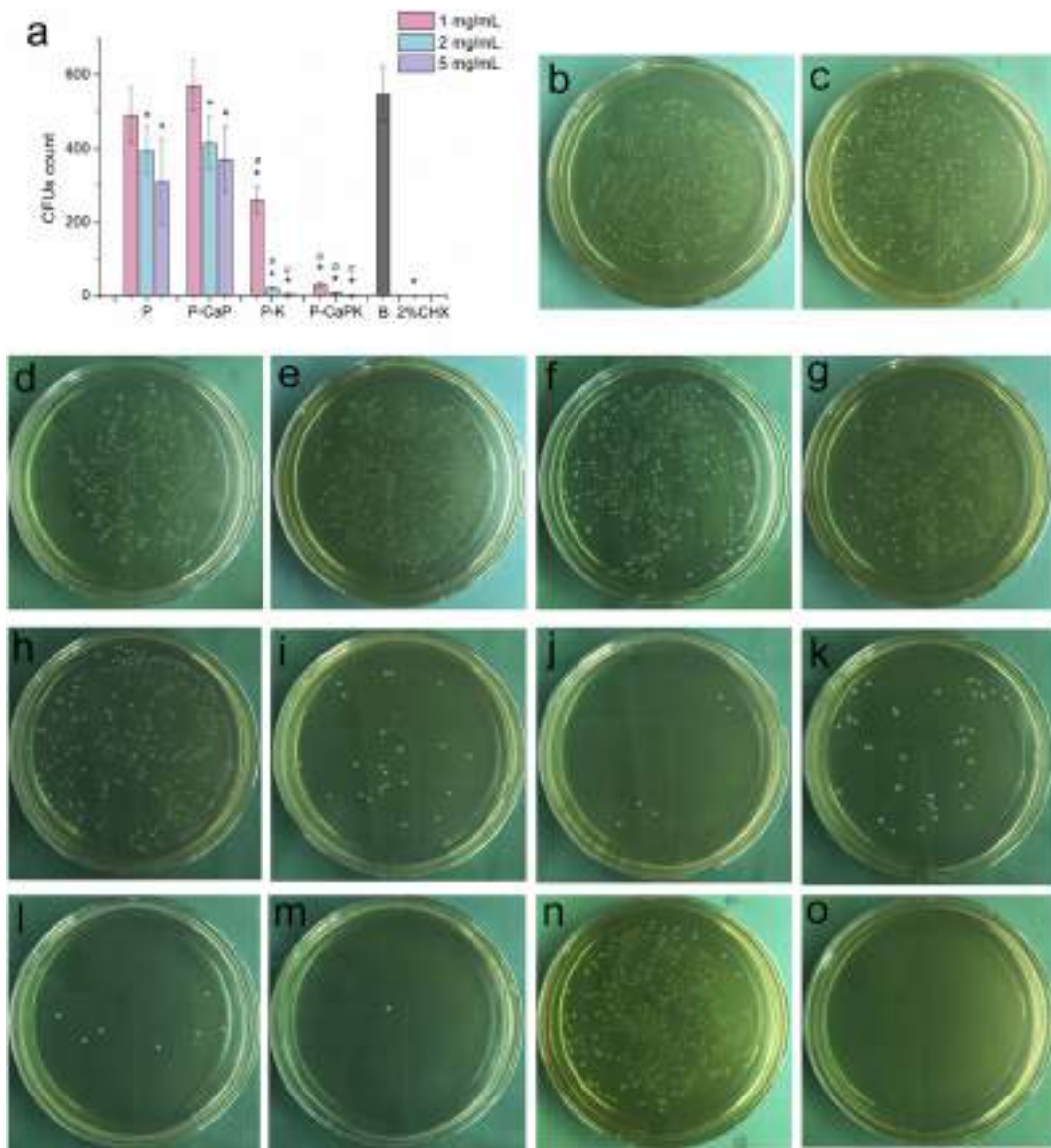
Fig. 4. Antibacterial effects of P, P-CaP, P−K and P-CaPK against planktonic *E. faecalis*. a. comparison of CFUs count among groups; b, c, d. representative images of CFUs of 1 (b), 2 (c), 5 (d) mg/mL of P; e, f, g. representative images of CFUs of 1 (e), 2 (f), 5 (g) mg/mL of P-CaP; h, i, j. representative images of CFUs of 1 (h), 2 (i), 5 (j) mg/mL of P-K; k, l, m. representative images of CFUs of 1 (k), 2 (l), 5 (m) mg/mL of P-CaPK; n. representative image of CFUs of negative control group; o. representative image of CFUs of 2% CHX group; B: negative control group; *: $p < 0.05$ compared with negative control group; *a, b, c*: $p < 0.05$ between the groups with the same label.
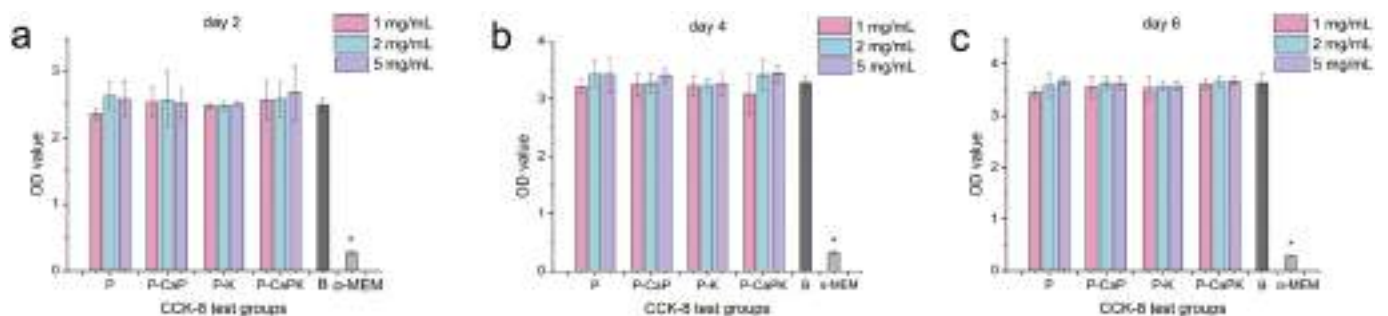
Fig. 5. CCK-8 results of biotoxicity. a. CCK-8 test result with culture time of 2 days; b. CCK-8 test result with culture time of 4 days; c. CCK-8 test result with culture time of 6 days; B: cell culture group without adding extracts; α-MEM: medium background; columns in pink color: cell culture group with 1 mg/mL of particles extracts; columns in blue color: cell culture group with 2 mg/mL of particles extracts; columns in purple color: cell culture group with 5 mg/mL of particles extracts;*: $p < 0.05$. (For interpretation of the references to color in this figure legend, the reader is referred to the web version of this article.)
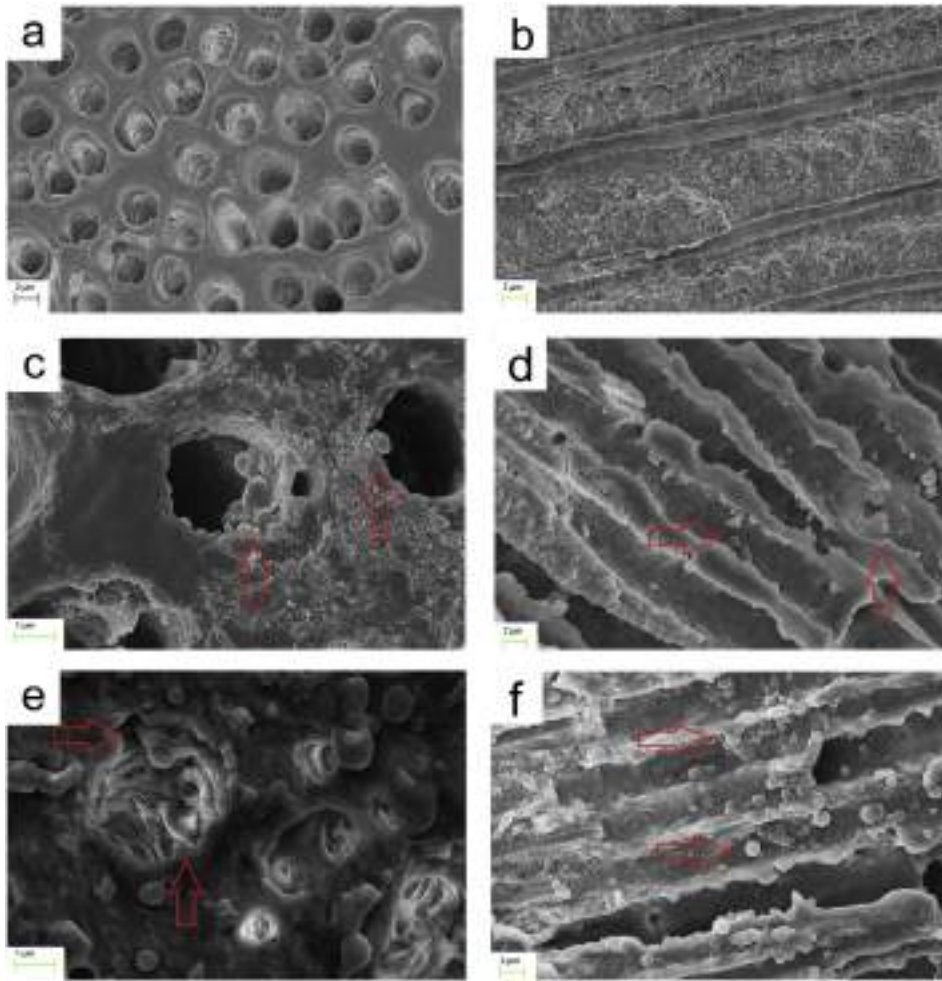
Fig. 6. Infiltration of P−K and P-CaPK into dentinal tubules. a. original dentinal tubule orifices; b. original axial cross-section of dentinal tubules; c. dentinal tubule orifices after P−K medication; d. axial cross-sections of dentinal tubules after P−K medication; e. dentinal tubule orifices after P-CaPK medication; f. axial cross-sections of dentinal tubules after P-CaPK medication; arrows indicating particles inside the tubules.

The dogs were sacrificed after 8 weeks by intravenous injection of an overdose of pentobarbital sodium. Postoperative periapical radiographs were also taken. The mandibles were dissected and sectioned after perfusion of NS and 4% paraformaldehyde. The experimental teeth with surrounding alveolar bone were fixed, decalcified, dehydrated, cleared and embedded in paraffin. Seven micrometer-thick sections were obtained and stained with hematoxylin and eosin (H&E). Sections were observed using a light microscope (BX53, Olympus Corporation, Japan) and evaluated based on the parameters described below [45]:

(i) Inflammatory infiltrate — dense infiltration zone was defined as an area with intense inflammatory cells and collagen degradation. Normal (score 1), mild (area of dense infiltration zone in periapical lesion < 30%, score 2), moderate (area of dense infiltration zone in periapical lesion > 30% and < 50%, score 3), severe (area of dense infiltration zone in periapical lesion > 50%, score 4);

(ii) Thickness of periodontal ligament — normal (score 1), slightly increased (the widest periodontal ligament space is within 3 times of the normal periodontal ligament thickness, score 2), moderately increased (the widest periodontal ligament space is 3–5 times of the normal periodontal ligament thickness, score 3), severely increased (the widest periodontal ligament space is > 5 times of the normal periodontal ligament thickness, score 4);

(iii) Resorption of mineralized tissues—absent (score 1), present (score 2).

The number and area of the radiolucent zone around the root apex in the radiographic images were also measured and analyzed. The ImageJ software (National Institutes of Health, Bethesda, MD, USA) was used for measurement. In addition, the sections were also stained by Brown and Brenn technique (American MasterTech, Lodi, CA, USA) for evaluation of bacteria distribution. The TRAP staining kit (MilliporeSigma) was used to stain osteoclast cells; the number of osteoclasts within 4×4 mm^2 around the root apex was counted.

2.10. Statistical analysis

Analysis of quantifiable data was performed parametrically using one-way analysis of variance and post-hoc Student-Newman-Keul test after validating the normality and homoscedasticity assumptions of the data sets. If those assumptions were violated, non-parametric analyses were performed using the Kruskal-Wallis analysis of variance and post-hoc Dunn's test. Statistical analysis was performed using the SPSS software (IBM, Armonk, NY, USA). For enumeration data, t statistical analysis was conducted using the Fisher exact test with Bonferroni correction. Statistical significance was preset at $\alpha = 0.05$.

3. Results

Scanning electron microscopy showed that P, P-CaP, P−K and P-CaPK all have spherical shapes with smooth surfaces (Fig. 2a, d, g, j). Elemental analysis indicated that P and P-CaP contained carbon and
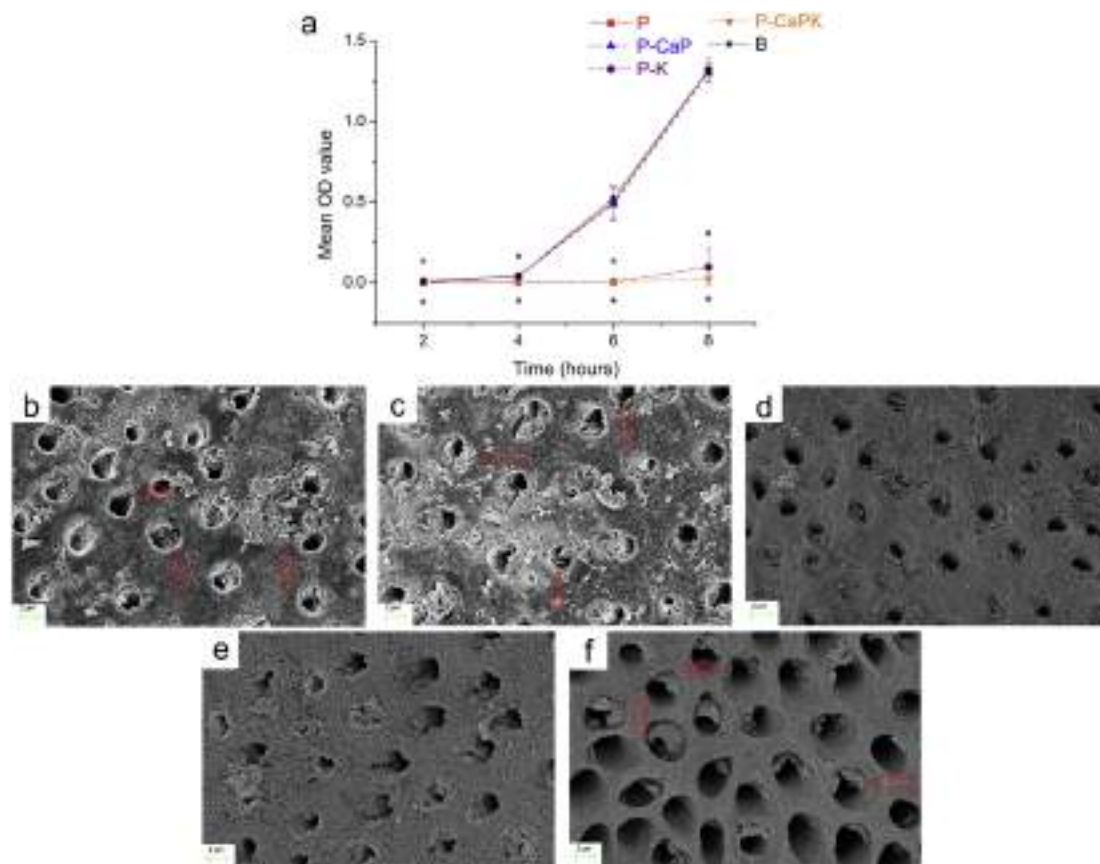
Fig. 7. Inhibition of *E. faecalis* on dentin. a. the curve of OD value within 8 h after the immersion of dentin slices into fresh BHI solution; b. *E. faecalis* growth on dentin slice of P group; c. *E. faecalis* growth on dentin slice of P-CaP group; d. *E. faecalis* growth on dentin slice of P−K group; e. *E. faecalis* growth on dentin slice of P-CaPK group; f. *E. faecalis* growth on dentin slice of negative control group; arrows indicating bacteria; *: $p < 0.05$.

oxygen elements while P−K and P-CaPK contained carbon, oxygen, silicon and chlorine (Fig. 2b, e, h, k). Table 2 listed the specific percentage of different elements in the submicron particles. The diameter of particles measured by DLS was also summarized in Table 2. The diameters of P and P-CaP were 727.97 ± 71.52 nm and 647.20 ± 75.70 nm, respectively, while the diameters of P−K and P-CaPK were much lower (256.43 ± 10.75 nm and 256.37 ± 29.81 nm). Compared with P−K, P-CaPK displayed increased uniformity of size distribution (Fig. 2i, l). Incorporation of K21 reversed the negative zeta potential of the submicron particles. The zeta potentials of P−K and P-CaPK were 35.67 ± 1.11 mV and 33.97 ± 1.62 mV, respectively, which were higher than those of P and P-CaP.

Infrared spectra of P, P-CaP, P−K and P-CaPK showed enhanced adsorption peaks at 2920 and 2852 cm^{-1} in P−K and P-CaPK group. This could be attributed to the methylene (-CH$_2$) and methyl groups (-CH$_3$) of the K21 molecule. The bands observed at 1761 cm^{-1} of all particles corresponded to carbonyl groups (C=O) in PLGA. The enhanced adsorption peak at 3427 cm^{-1} of P−K and P-CaPK was assigned to the specific adsorption peak of the hydroxyl groups (-OH) of the K21 molecule (Fig. 2m). The EE and LC of calcium, phosphorus and K21 were listed in Table 3. For calcium and phosphorus, the EE and LC in P-CaP were higher than those in P-CaPK. Calcium had a slightly higher EE than phosphorus while K21 had the highest EE.

The P, P-CaP, P−K and P-CaPK particles were all acidic when dispersed in dd H$_2$O. At the early stage, the pH values of P−K and P-CaPK were similar but lower than those of P and P-CaP. The pH values of different solutions approximated each other and reached 2.6 at the end of soaking time (Fig. 3a). Both calcium and phosphorus were released in a sustained manner from P-CaP and P-CaPK after immersion in Tris-

HCl. The total amount of released calcium was higher than that of phosphorus. The releasing rate of calcium was relatively constant during the 27-day period, while phosphorus was released fast during the first 9 days (Fig. 3b, c). The release of K21 could be detected spectrophotometrically. P-CaPK released more K21 than P−K. The releasing rate of K21 from P−K was relatively stable while P-CaPK released K21 at a variable rate over time (Fig. 3d).

Both P−K and P-CaPK submicron particles exhibited potent antibacterial activity against *E. faecalis* at all concentrations and the effects were particularly strong when the concentrations of particles were 2 and 5 mg/mL. P-CaPK showed stronger bactericidal ability than P−K at the same concentration. P and P-CaP also demonstrated slight antimicrobial activity at 2 and 5 mg/mL. The 2% CHX positive control completely inhibited the growth of *E. faecalis* (Fig. 4; $p < 0.05$). Irrespective of the different concentrations and exposure times, P, P-CaP, P−K and P-CaPK had no suppressive effect on the proliferation of MC3T3-E1 cells when compared with control groups (Fig. 5; $p > 0.05$).

Residual submicron particles were present on the dentin slices after ultrasonic vibration of the P−K and P-CaPK suspensions. Some particles appeared to have agglomerated. Both P−K and P-CaPK particles infiltrated the dentinal tubules after ultrasonic activation (Fig. 6). For inhibition of *E. faecalis* grown on dentin, the OD values of the P and P-CaP groups were not significantly different from the control group at all time points. However, the OD values of the P−K and P-CaPK groups were significantly lower than the other groups at different time points (Fig. 7a). Scanning electron microscopy showed that submicron particles remained on the dentin surfaces of all experimental groups. Dentin slices treated with P and P-CaP showed bacteria attachment while slices treated with P−K and P-CaPK showed negligible bacteria growth
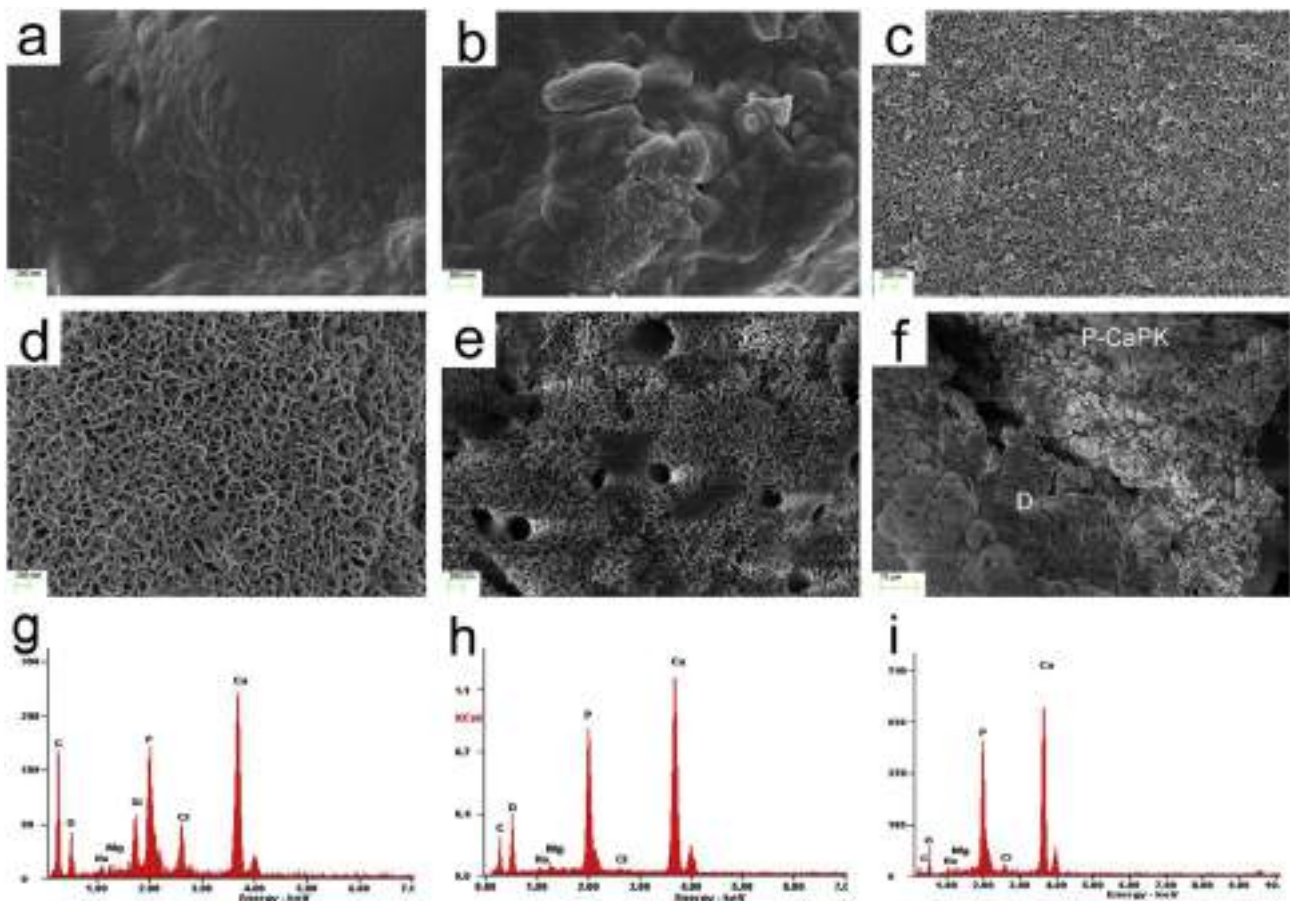
Fig. 8. *In vitro* mineralization of different groups. a. surface of P after immersion in SBF; b. surface of P-CaP after immersion in SBF; c. surface of P−K after immersion in SBF; d. surface of P-CaPK after immersion in SBF; e. surface of dentin after immersion in SBF; f. connection between crystals on the surface of P-CaPK and dentin; g. EDS analysis of crystals on the surface of P-K; h. EDS analysis of crystals on the surface of P-CaPK; i. EDS analysis of crystals on the surface of dentin. D: dentin.

(Fig. 7b–f).

With respect to the capacity for mineralization, particles from the P and P-CaP groups degraded rapidly and lost their spherical shape after immersion in SBF for 3 weeks (Fig. 8a, b). In contrast, innumerous needle-like crystallites were present on the surface of the P-CaPK particles while only limited crystallites were formed on the surface of the P−K particles (Fig. 8c, d). Elemental analysis indicated that the composition of the crystallites on the P-CaPK particles was consistent with that of hydroxyapatite. Crystallites on the surface of the P−K particles also contained silicon and chlorine elements (Fig. 8g, h). Hydroxyapatite crystallites were present on the surfaces of the adjacent dentin in all groups (Fig. 8e, i). Crystallites formed on the surface of the P-CaPK particles appeared to have merged with those present on the dentin surface (Fig. 8f).

Radiolucent zones were identified in the periapical region of the beagle dogs' teeth after 8 weeks of *E. faecalis* incubation. The incidence of formation of these radiolucent zones was: 30% for the 2% CHX group, 55.6% for the P-CaPK group, 90% for the CH group and 90% for NS group. The difference between 2% CHX group and the other groups was statistically significant (Fig. 9a). There was no significant difference in the mean area of the radiolucent zone among all groups (Fig. 9b). Although no significant difference was observed, the P-CaPK group displayed less number of roots with radiolucent zones. There was no obvious radiolucent zone in the radiographic images of specimens derived from the 2% CHX group and the P-CaPK group (Fig. 9c, d, g, h). In contrast, radiolucent zones could be identified from radiographic images of specimens derived from the CH group and the NS group (Fig. 9e, f, i, j).

Hematoxylin and eosin-stained sections were evaluated from three aspects: inflammatory infiltrate, thickness of periodontal ligament and resorption of mineralized tissues. In terms of inflammatory infiltrate, the result of NS group was quite uniform with 90% of the specimens showing severe inflammatory infiltrate. There was no significant difference between the NS group and the 2% CHX group or the CH group ($p > 0.05$). Only the P-CaPK group exhibited mild inflammatory infiltrate. The 2% CHX group showed the most variable tissue response among the specimens (Fig. 10a). There was no significant difference in the thickness of the periodontal ligament among all groups. Sections of both NS and P-CaPK groups displayed moderately or severely increased periodontal ligament space, while sections of the 2% CHX group and CH group showed big differences within groups (Fig. 10b).

All specimens from the NS group and P-CaPK group showed resorption of mineralized tissues in the periapical region. There was no resorption of mineralized tissues in one specimen from the CH group and 40% of the specimens from the 2% CHX group. A significant difference was observed between the 2% CHX group and the NS group (Fig. 10c). Considering all three aspects of histologic evaluation, a significant difference was found between the NS group and the 2% CHX group or the P-CaPK group. The P-CaPK group and the NS group showed more homogeneous tissue responses among specimens within the group (Fig. 10d).

Representative images of H&E-stained sections from the different groups are shown in Fig. 11. Sections from the 2% CHX group showed almost no inflammatory infiltrate and destruction of the periodontal ligament, with normal structure of the periapical tissues (Fig. 11a). Mild inflammatory infiltrate, moderately increased periodontal ligament space with resorption of the periapical mineralized tissues could be identified from the sections prepared from the P-CaPK group
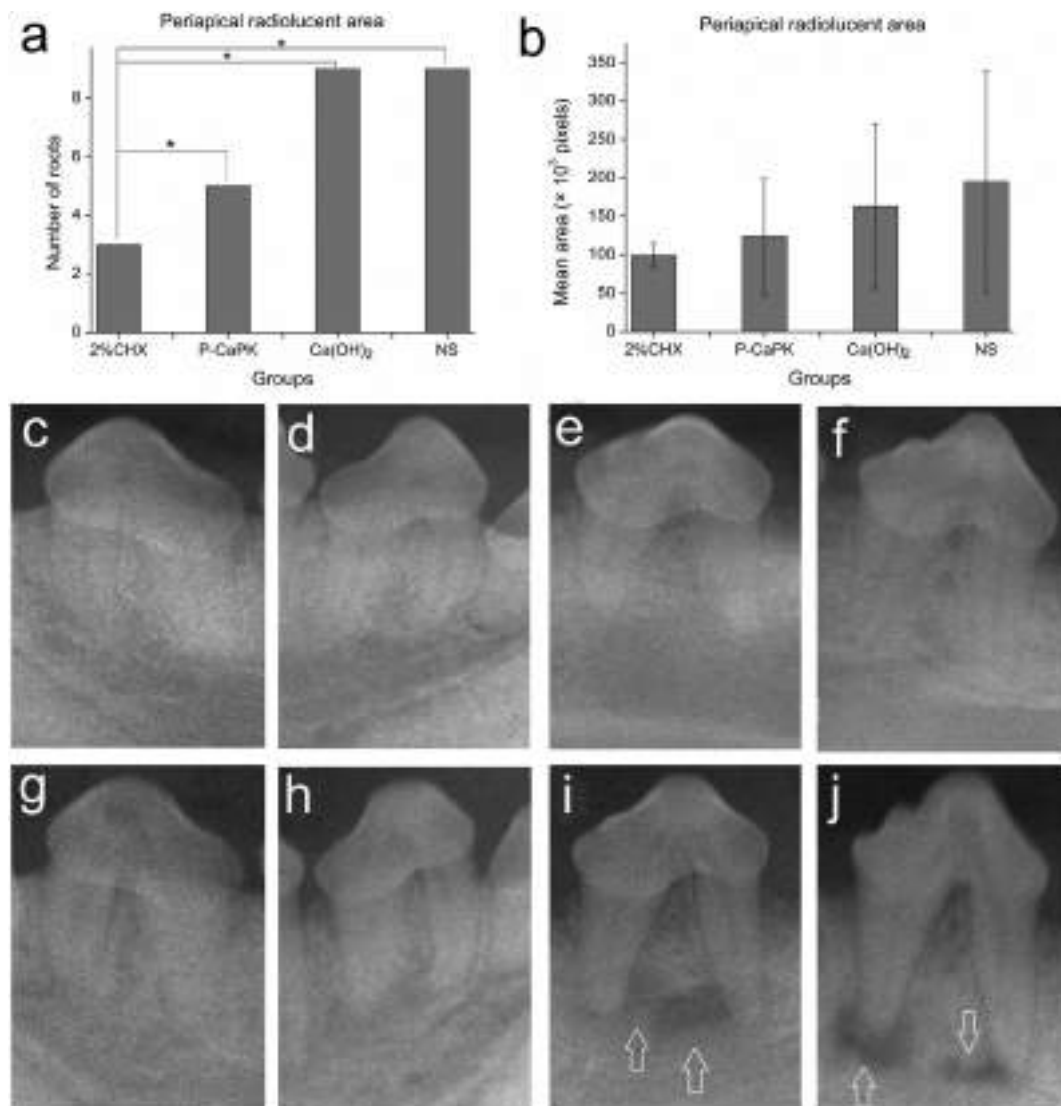
Fig. 9. Radiographic evaluation of apical lesions. a. comparison of number of roots with apical radiolucent area; b. comparison of mean areas of apical radiolucent area; c, g. preoperative and postoperative radiographs of 2% CHX group; d, h. preoperative and postoperative radiographs of P-CaPK group; e, i. preoperative and postoperative radiographs of CH group; f, j. preoperative and postoperative radiographs of NS group; arrows indicating the apical radiolucent area; *: $p < 0.05$.

(Fig. 11b). Specimens from the CH group and NS group both showed severe inflammatory infiltrate as well as destruction of periodontal ligament and periapical bone tissues (Fig. 11c, d).

Bacterial staining with the Brown and Brenn technique revealed bacterial growth on the canal wall as well as within the dentinal tubules. Sections from the CH group and NS group demonstrated extensive bacteria infiltration into the dentinal tubules (up to 1500 μm) as well as the root apical tissues (Fig. 12c–f). In contrast, less bacteria could be identified in the dentinal tubules of the 2% CHX and the P-CaPK groups (Fig. 12a, b).

There was a significant difference between the P-CaPK group and the NS group in the number of TRAP-positive osteoclasts (Fig. 13a). The distribution of osteoclasts was extensive within the periapical trabecular bone and root apices in the 2% CHX, CH and NS groups. Sections prepared from the P-CaPK group demonstrated the least number of osteoclasts (Fig. 13b–i).

4. Discussion

In the present study, K21, calcium and phosphorus elements were successfully incorporated into PLGA submicron particles using emulsion-solvent evaporation method, which was confirmed by EDS, FTIR and release profiles. Calcium and phosphorus could not be detected with EDS, probably due to their low loading content. Incorporation of K21 affected both the size distribution and zeta potential of the submicron particles. Compared with P and P-CaP, the diameter of the P−K and P-CaPK particles decreased while the zeta potential changed to positive values. Because both the dentin surface and bacteria cell membranes are negatively-charged [46], particles with positive zeta potential are likely to interact much easier with dentin and bacteria than particles with negative zeta potential.

In the presence of water, PLGA polymers hydrolyzed and produced lactic and glycolic acids, resulting in the low pH values. Acid conditions might inhibit bacteria growth by increasing the hydrogen-ion concentration in the microorganism [47]. The pH values of the P−K and P-CaPK particles were lower in dd H_2O than the P and P-CaP particles during the early stage but became similar to each other toward the end of the experiment. This was possibly caused by the release of K21, which accelerated the degradation of PLGA polymer. It had been reported that some enzymes, free radicals and/or acid-based products of biological compounds can speed up PLGA degradation [48]. The degradation rate may be regulated by modulating the concentration of
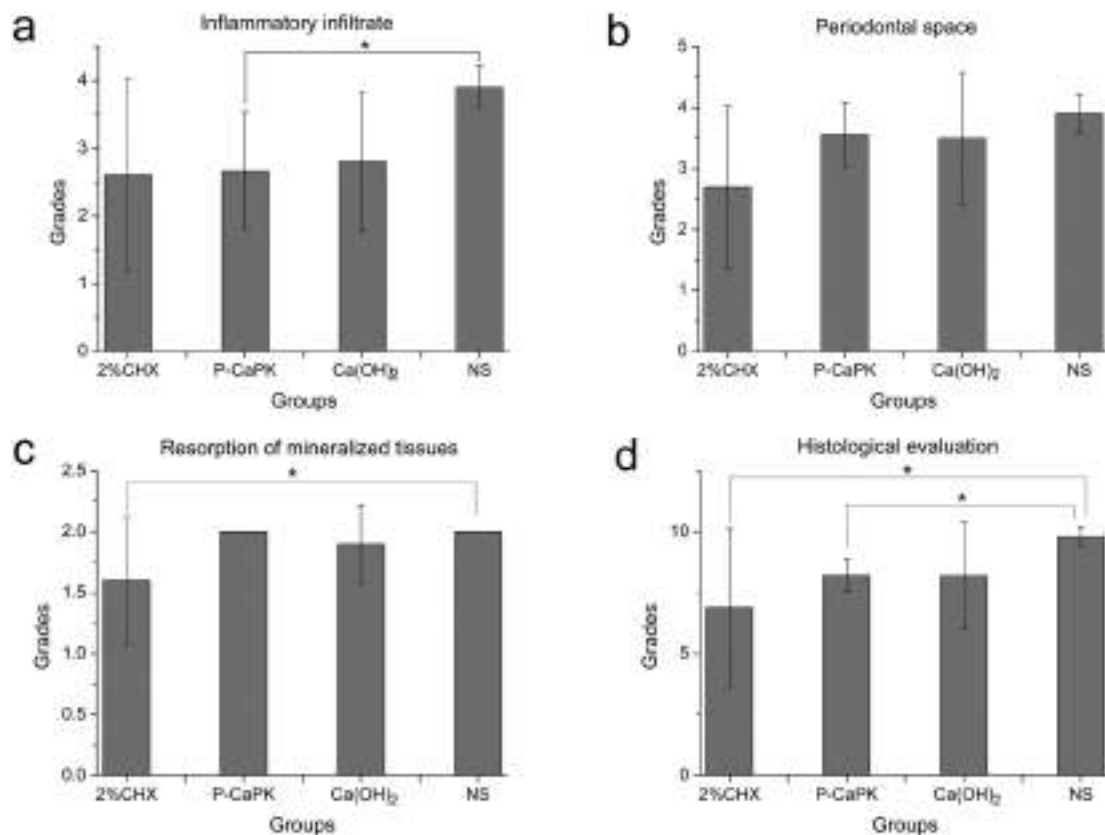
Fig. 10. Histological evaluation of apical lesions. a. inflammatory infiltrate; b. periodontal space; c. resorption of mineralized tissues; d. comprehensive evaluation; *: $p < 0.05$.

these products around PLGA systems [48]. In Tris-HCl, both calcium and phosphorus were released in a sustained manner. Inclusion of K21 did not interfere with the incorporation and release of calcium and phosphorus. However, the amount and rate of release of K21 differed in P−K and P-CaPK. It is speculated that the release of calcium and phosphorus promoted the release of K21. This phenomenon may be related to the difference in binding site and form between PLGA, K21, calcium and phosphorus.

When cultured with planktonic *E. faecalis*, P−K and P-CaPK at different concentrations all displayed remarkable dose-dependent antibacterial activities. Growth of *E. faecalis* was almost completely inhibited when the particles were at a concentration of 5 mg/mL. The P-CaPK group demonstrated more potent antimicrobial activity compared with the P−K group at the same concentration. Based on the K21 release test result, this difference may be accounted for by the difference in the released amount of K21 in the bacteria suspensions. In a recent study on coating of surgical sutures and dental floss with K21 solutions, a K21 coating endowed the sutures and dental floss with antimicrobial activity against *Porphyromonas gingivalis* and *E. faecalis* in a dose-dependent manner [49]. In the present work, P−K and P-CaPK submicron particles successfully infiltrated into dentinal tubules of dentin slices after ultrasonic activation and both demonstrated inhibitory effects on bacteria growth. According to SEM images, there were almost no bacteria attachment on the dentin slices. Submicron and nano structure would enable biomaterials to possess better penetration ability [50]. Besides, as mentioned before, dentin was negatively charged. Thus, the small size of particles and positive zeta potential may have contributed to better dispersion, infiltration and substantivity on dentin.

Submicron particles derived from the P, P-CaP, P−K and P-CaPK groups at different concentrations all exhibited no suppressive effect on the proliferation of MC3T3-E1 cells despite different co-culture times. Human dental pulpal cells have previously been seeded on dentin discs

prior to the application of K21 to evaluate the biocompatibility of K21 [22]. The authors found that K21 was only mildly cytotoxic and had better cell viability compared with 2% CHX. The CHX is a cationic surfactant and its dose-dependent cytotoxicity of CHX has been well proved [51]. In our pilot experiments, K21 solution was incorporated into PLGA polymers at higher concentrations. However, improvements in antimicrobial activity were accompanied by increases in cytotoxicity. Hence, PLGA was used as a carrier for 20% K21 to strike a balance between biocompatibility and antibacterial activity.

The osteogenic bioactivity of a material may be evaluated by examining the formation of apatite on its surface after immersion in SBF. In general, apatite crystallite is formed on the surface of bone filling materials within four weeks [44]. In the present study, P and P-CaP particles degraded without crystallite formation after immersion in SBF for three weeks; the results indicate that PLGA submicron particles alone do not possess mineralization induction potential. In contrast, abundant apatite crystallites were deposited on the surface of the P-CaPK particles. Indeed, the P-CaPK group demonstrated better *in vitro* mineralization than the P−K group. It was previously reported that K21 inhibits endogenous matrix metalloproteinases and cysteine cathepsins, thereby increasing the resistance of dentin collagen against degradation [52]. Although K21 *per se* does not promote the formation of mineralized tissues, the silicon element in the K21 may possibly act as nucleation substrate for calcium and phosphorus during the early stage of mineralization [53]. According to literature, silicon, calcium and phosphorus are all essential for mineralization and osteogenesis both *in vitro* and *in vivo* [54–56]. In root canals, deposition of apatite crystallites on the canal wall may help block dentinal tubules, thereby preventing bacteria invasion [57]. In periapical defects, apatite-like crystallites formed on the surface of biomaterials promote the bonding of these materials to the surrounding bone tissues, and facilitate the restoration of defects produced by bone resorption [58].
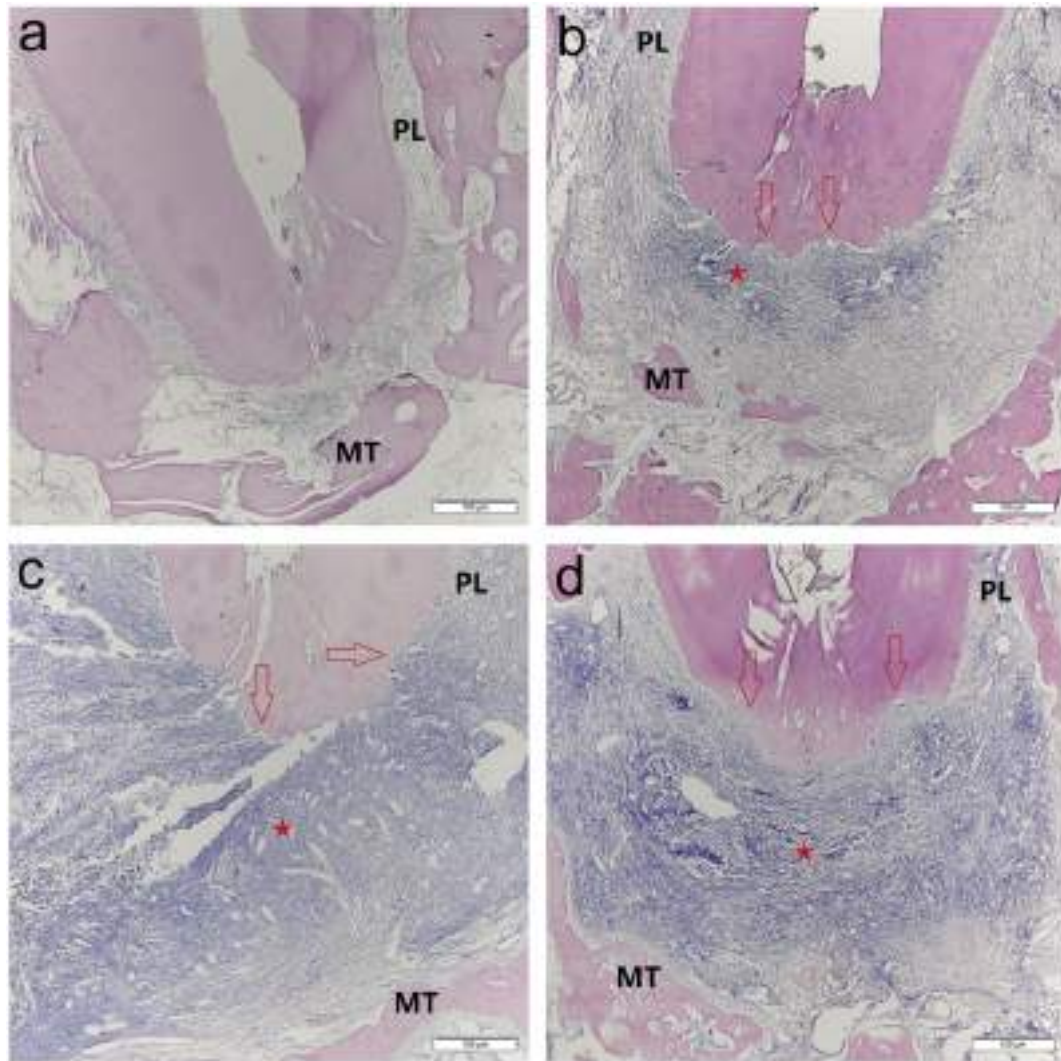
Fig. 11. Representative images of HE staining (×4). a. 2% CHX group; b. P-CaPK group; c. CH group; d. NS group; ★: dense inflammatory infiltrate zone; PL: periodontal ligament space; MT: mineralized tissues; arrows indicating root resorption.

Beagle dogs were often used as animal models for evaluation of root canal disinfectants and root-end filling materials [59,60]. In previous publications, experimental apical periodontitis was successfully induced in beagle dogs after pulp exposure for four to six weeks [61,62]. In the present study, the root canals were infected with a single species (E. faecalis) for eight weeks to establish apical periodontitis. After four weeks of E. faecalis infection, radiolucent areas around the root apex were visible in some specimens and the difference became more obvious with time. The periapical lesions in some specimens became clearer after eight weeks of infection.

Only 2% CHX significantly decreased the size of the periapical lesions when evaluation was based on radiographic interpretation alone. Although all specimens from the P-CaPK group showed different extents of periapical bone tissue destruction, resorption was limited or mild in some specimens and was not detected from the radiographs. When the radiographic and histological results were evaluated together, 2% CHX was capable of reducing the resorption of mineralized tissues and displayed the strongest inhibitive effect against E. faecalis. Particles from the P-CaPK group decreased the propensity of inflammatory infiltrate in the periapical tissues but were ineffective in preventing resorption of mineralized tissue and widening of the periodontal space. Particles from the CH group were similar to the effects of NS, in that they could not prevent infection of E. faecalis. In vitro studies reported that calcium hydroxide is only weakly effective as an intracanal medicament against

E. faecalis [63,64]. In addition, calcium hydroxide possesses negligible substantivity and infiltrates dentinal tubules poorly [65]. In a previous study, different calcium hydroxide-based intracanal dressings were placed in dogs' teeth with periapical lesions, and the distribution of microorganisms in root canal systems was examined after 21 days [66]. The percentage of sites containing microorganisms was between 62%–87% for all groups. Mechanical canal preparation combined with CH paste did not effectively eliminate infection from the root canal systems. In another study, the antimicrobial effects of different irrigating solutions were investigated in the root canals of dogs' teeth [67]. The saline group and the control group contained an increased number of microorganisms while there was reduction in the number of microorganisms in the NaOCl and CHX groups. Results from the present work were consistent with these studies.

Brown and Brenn staining was often performed to observe the presence of bacteria in tissue sections [46,68]. It has been suggested that E. faecalis invades dentinal tubules to escape from root canal disinfectants [69]. Invasion of E. faecalis into dentinal tubules was also detected in the present study. Sections derived from the CHX and P-CaPK groups demonstrated less extensive bacteria infiltration. The substantivity of CHX on dentin and the infiltration ability of P-CaPK probably contributed to the prevention of bacteria invasion. TRAP staining was applied for the evaluation of osteoclast cells [70]. Compared with NS, P-CaPK reduced the number of osteoclasts significantly.
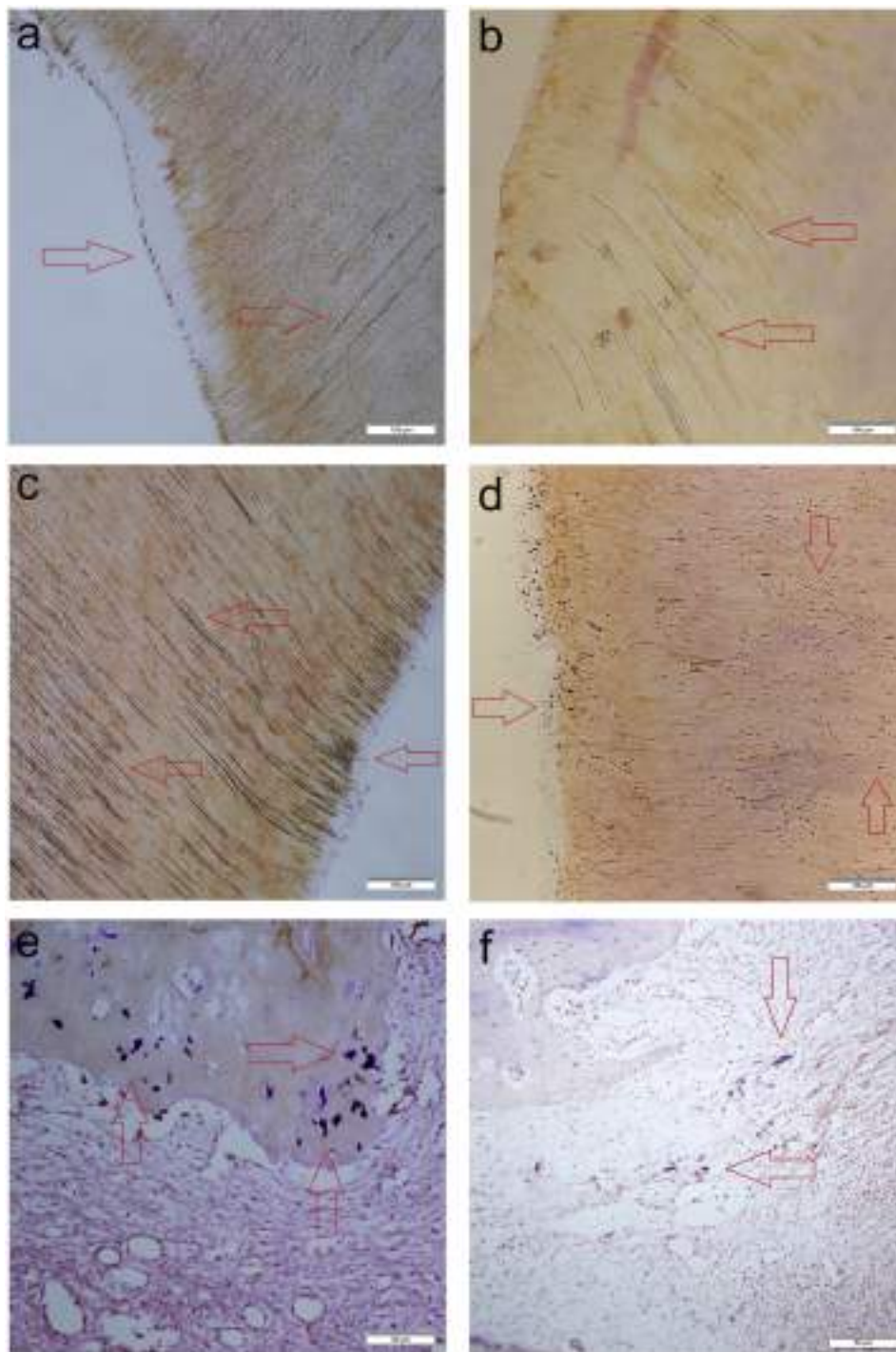
Fig. 12. Representative images of Brown and Brenn staining. a. root canal wall of 2% CHX group (×10); b. root canal wall of P-CaPK group (×10); c. root canal wall of CH group (×10); d. root canal wall of NS group (×10); e. root apex of NS group (×20); f. periapical region of CH group (×20); arrows indicating bacteria.

pH measurement indicated that P-CaPK is acidic. It has been reported that acidic condition inhibits osteoclast differentiation and proliferation, but increases the resorptive activity of differentiated osteoclasts [71]. The number of osteoclasts in the P-CaPK group was less than that of the NS group, but there was no significant difference in terms of resorption of mineralized tissues. Although mineralized tissues resorption was not severe in some of 2% CHX specimens, a relatively intense distribution of osteoclasts could still be observed in the periapical trabecular bone. The reason for this phenomenon is unknown and requires further investigation.

Based on the findings of the present study, P-CaPK possesses

excellent antimicrobial and mineralization ability and inhibits *E. faecalis* infection of teeth *in vitro* and *in vivo*. Although CHX has stronger antibacterial activity, it has more severe cytotoxicity and does not possess mineralization potential [51,72]. The P-CaPK shows promise to be developed into a new intracanal disinfectant for root canal treatment.

5. Conclusions

Submicron P-CaPK particles were fabricated and showed excellent antibacterial activity, good biocompatibility, *in vitro* mineralization
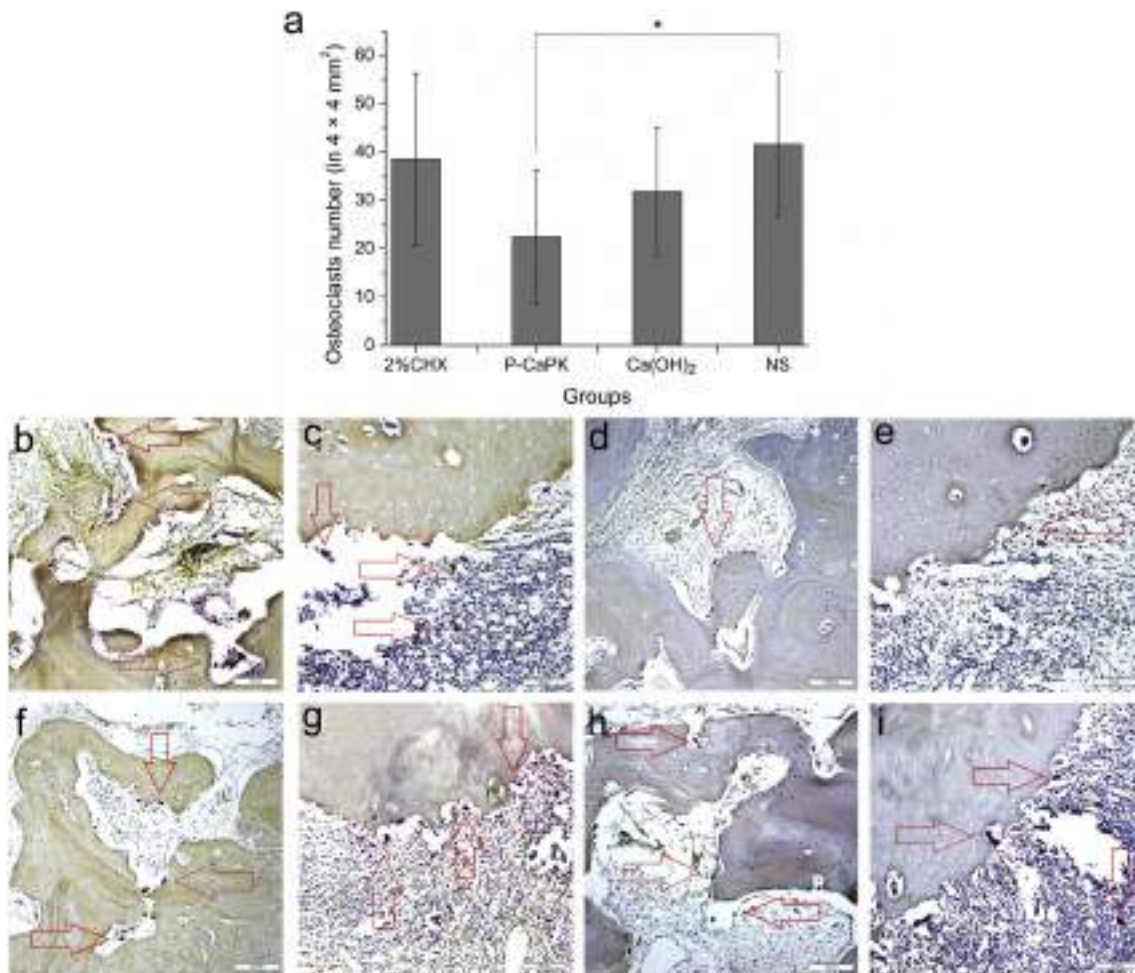
Fig. 13. TRAP staining of root apical samples from different groups. a. comparison of osteoclasts among groups; b. osteoclasts of 2% CHX group in periapical trabecular bone ($\times 10$); c. osteoclasts of 2% CHX group around the root apex ($\times 20$); d. osteoclasts of P-CaPK group in periapical trabecular bone ($\times 10$); e. osteoclasts of P-CaPK group around the root apex ($\times 20$); f. osteoclasts of CH group in periapical trabecular bone ($\times 10$); g. osteoclasts of CH group around the root apex ($\times 20$); h. osteoclasts of NS group in periapical trabecular bone ($\times 10$); i. osteoclasts of NS group around the root apex ($\times 20$); arrows indicating osteoclasts; *: $p < 0.05$.

potential and infiltrated well into the dentinal tubules. These submicron particles also demonstrated a strong preventive effect against *E. faecalis* infection in root canals of teeth *in vivo*. Due to the biodegradability, P-CaPK might be developed into a new effective disinfectant for infected root canals as an intermediate medication. However, further issues have to be clarified before its clinical applications, such as influences on the root canal sealing and other intra-canal chemicals.

Declaration of competing interest

The authors declare that they have no known competing financial interests or personal relationships that could have appeared to influence the work reported in this paper.

Acknowledgments

References

[1] I. Prada, P. Micó-Muñoz, T. Giner-Lluesma, P. Micó-Martínez, N. Collado-Castellano, A. Manzano-Saiz, Influence of microbiology on endodontic failure. Literature review, Med. Oral Patol. Oral Cir. Bucal. 24 (3) (2019) e364–e372.

[2] A.P. Sobrinho, M.H. Barros, J.R. Nicoli, M.A. Carvalho, L.M. Farias, E.A. Bambirra, M.G. Bahia, E.C. Vieira, Experimental root canal infections in conventional and germ-free mice, J Endod 24 (6) (1998) 405–408.

[3] S. George, A. Kishen, P. Song, The role of environmental changes on monospecies biofilm formation on root canal wall by *Enterococcus faecalis*, J Endod 31 (12) (2005) 867–872.

[4] T.K. Madsen, M.N. Skov, S. Gill, M. Kemp, Virulence factors associated with *Enterococcus faecalis* infective endocarditis: a mini review, Open Microbiol J 11 (2017) 1–11.

[5] G. Kayaoglu, D. Ørstavik, Virulence factors of *Enterococcus faecalis* relationship to endodontic disease, Crit. Rev. Oral Biol. Med. 15 (2004) 308–320.

[6] P. Diogo, C. Fernandes, F. Caramelo, M. Mota, I.M. Miranda, M.A.F. Faustino, M.G.P.M.S. Neves, M.P. Uliana, K.T. de Oliveira, J.M. Santos, T. Gonçalves, Antimicrobial photodynamic therapy against endodontic *Enterococcus faecalis* and *Candida albicans* mono and mixed biofilms in the presence of photosensitizers: a comparative study with classical endodontic irrigants, Front. Microbiol. 8 (2017) 498.

[7] F. Sabouni, Z. Movahedi, S. Mahmoudi, B. Pourakbari, S. Keshavarz Valian, S. Mamishi, High frequency of vancomycin resistant *Enterococcus faecalis* in children: an alarming concern, J Prev Med Hyg 57 (4) (2016) E201–E204.

[8] A. Dahl, N.E. Bruun, *Enterococcus faecalis* infective endocarditis: focus on clinical aspects, Expert. Rev. Cardiovasc. Ther. 11 (9) (2013) 1247–1257.

[9] C.L. Hall, B.L. Lytle, D. Jensen, J.S. Hoff, F.C. Peterson, B.F. Volkman, C.J. Kristich, Structure and dimerization of IreB, a negative regulator of cephalosporin resistance in *Enterococcus faecalis*, J. Mol. Biol. 429 (15) (2017) 2324–2336.

[10] P. Louwakul, A. Saelo, S. Khemaleelakul, Efficacy of calcium oxide and calcium hydroxide nanoparticles on the elimination of *Enterococcus faecalis* in human root dentin, Clin. Oral Investig. 21 (3) (2016) 865–871.

[11] V. Peciuliene, I. Balciuniene, H.M. Eriksen, M. Haapasalo, Isolation of *Enterococcus faecalis* in previously root-filled canals in a Lithuanian population, J Endod 26 (10) (2000) 593–595.

[12] D.T.S. Wong, G.S.P. Cheung, Extension of bactericidal effect of sodium hypochlorite into dentinal tubules, J Endod 40 (6) (2014) 825–829.

[13] D. Deniz Sungur, H. Aksel, N. Purali, Effect of a low surface tension vehicle on the dentinal tubule penetration of calcium hydroxide and triple antibiotic paste, J

Endod 43 (3) (2017) 452–455.

[14] W. Fan, Q. Sun, Y. Li, F.R. Tay, B. Fan, Synergistic mechanism of Ag$^+$-Zn^{2+} in antibacterial activity against *Enterococcus faecalis* and its application against dentin infection, J nanobiotechnol 16 (1) (2018) 10.

[15] M. Al-Zubidi, M. Widziolek, E.K. Court, A.F. Gains, R.E. Smith, K. Ansbro, A. Alrafaie, C. Evans, C. Murdoch, S. Mesnage, C.W.I. Douglas, A. Rawlinson, G.P. Stafford, Identification of novel bacteriophages with therapeutic potential that target *Enterococcus faecalis*, Infect. Immun. 87 (11) (2019) e00512–e00519.

[16] L. Khalifa, Y. Brosh, D. Gelman, S. Coppenhagen-Glazer, S. Beyth, R. Poradosu-Cohen, Y.A. Que, N. Beyth, R. Hazan, Targeting *Enterococcus faecalis* biofilms with phage therapy, Appl. Environ. Microbiol. 81 (8) (2015) 2696–2705.

[17] A.J. McBain, R.G. Ledder, L.E. Moore, C.E. Catrenich, P. Gilbert, Effects of quaternary-ammonium-based formulations on bacterial community dynamics and antimicrobial susceptibility, Appl. Environ. Microbiol. 70 (6) (2004) 3449–3456.

[18] Y. Xue, H. Xiao, Y. Zhang, Antimicrobial polymeric materials with quaternary ammonium and phosphonium salts, Int. J. Mol. Sci. 16 (2) (2015) 3626–3655.

[19] X. Chen, K. Cai, J. Fang, M. Lai, J. Li, Y. Hou, Z. Luo, Y. Hu, L. Tang, Dual action antibacterial TiO2 nanotubes incorporated with silver nanoparticles and coated with a quaternary ammonium salt (QAS), Surf Coat Tech 216 (2013) 158–165.

[20] L. Sun, Y. Du, L. Fan, X. Chen, J. Yang, Preparation, characterization and antimicrobial activity of quaternized carboxymethyl chitosan and application as pulp-cap, Polymer 47 (6) (2006) 1796–1804.

[21] F. Li, P. Wang, M.D. Weir, A.F. Fouad, H.H. Xu, Evaluation of antibacterial and remineralizing nanocomposite and adhesive in rat tooth cavity model, Acta Biomater. 10 (6) (2014) 2804–2813.

[22] D. Daood, C.K.Y. Yiu, M.F. Burrow, L.N. Niu, F.R. Tay, Effect of a novel quaternary ammonium silane cavity disinfectant on durability of resin-dentine bond, J. Dent. 60 (2017) 77–86.

[23] Y.P. Gou, J.Y. Li, M.M. Meghil, C.W. Cutler, H.H.K. Xu, F.R. Tay, L.N. Niu, Quaternary ammonium silane-based antibacterial and anti-proteolytic cavity cleanser, Dent. Mater. 34 (12) (2018) 1814–1827.

[24] N. Gulve, K. Kimmerling, A.D. Johnston, G.R. Krueger, D.V. Ablashi, B.K. Prusty, Anti-herpesviral effects of a novel broad range anti-microbial quaternary ammonium silane, K21, Antivir. Res. 131 (2016) 166–173.

[25] S. Nakamura, T. Matsumoto, J. Sasaki, H. Egusa, K.Y. Lee, T. Nakano, T. Sohmura, A. Nakahira, Effect of calcium ion concentrations on osteogenic differentiation and hematopoietic stem cell niche-related protein expression in osteoblasts, Tissue Eng Part A 16 (8) (2010) 2467–2473.

[26] B. Huang, L. Tan, X. Liu, J. Li, S. Wu, A facile fabrication of novel stuff with anti-bacterial property and osteogenic promotion utilizing red phosphorus and near-infrared light, Bioact Mater 4 (1) (2019) 17–21.

[27] E.A. Abou Neel, A. Aljabo, A. Strange, S. Ibrahim, M. Coathup, A.M. Young, L. Bozec, V. Mudera, Demineralization-remineralization dynamics in teeth and bone, Int. J. Nanomedicine 11 (2016) 4743–4763.

[28] Sunarso, R. Toita, K. Tsuru, K. Ishikawa, Immobilization of calcium and phosphate ions improves the osteoconductivity of titanium implants, Mater. Sci. Eng. C Mater. Biol. Appl. 68 (2016) 291–298.

[29] T. Tian, J. Liao, T. Zhou, S. Lin, T. Zhang, S.-R. Shi, X. Cai, Y. Lin, Fabrication of calcium phosphate microflowers and their extended application in bone regeneration, ACS Appl. Mater. Interfaces 9 (36) (2017) 30437–30447.

[30] M.K. Boushell, N.T. Khanarian, R.Z. LeGeros, H.H. Lu, Effect of ceramic calcium-phosphorus ratio on chondrocyte-mediated biosynthesis and mineralization, J. Biomed. Mater. Res. A 105 (10) (2017) 2694–2702.

[31] Z. Mladenovic, A. Sahlin-Platt, B. Andersson, A. Johansson, E. Bjorn, M. Ransjo, In vitro study of the biological interface of Bio-Oss: implications of the experimental setup, Clin. Oral Implants Res. 24 (3) (2013) 329–335.

[32] C. Wang, Y. Xue, K. Lin, J. Lu, J. Chang, J. Sun, The enhancement of bone regeneration by a combination of osteoconductivity and osteostimulation using beta-CaSiO₃/beta-Ca₃(PO₄)₂ composite bioceramics, Acta Biomater. 8 (1) (2012) 350–360.

[33] Q.W. Gao, P. Lan, H.L. Shao, X.C. Hu, Direct synthesis with melt polycondensation and microstructure analysis of poly(L-lactic acid-co-glycolic acid), Polym. J. 34 (11) (2002) 786–793.

[34] S. Kaihara, S. Matsumura, A.G. Mikos, J.P. Fisher, Synthesis of poly(L-lactide) and polyglycolide by ring-opening polymerization, Nat. Protoc. 2 (11) (2007) 2767–2771.

[35] H.X. Zhang, G.Y. Xiao, X. Wang, Z.G. Dong, Z.Y. Ma, L. Li, Y.H. Li, X. Pan, L. Nie, Biocompatibility and osteogenesis of calcium phosphate composite scaffolds containing simvastatin-loaded PLGA microspheres for bone tissue engineering, J. Biomed. Mater. Res. A 103 (10) (2015) 3250–3258.

[36] N.F. Hughes-Brittain, L. Qiu, W. Wang, T. Peijs, C.W.M. Bastiaansen, Degradation and biocompatibility of photoembossed PLGA-acrylate blend for improved cell adhesion, J Biomed Mater Res B Appl Biomater 106 (1) (2018) 163–171.

[37] N. Cui, J. Qian, J. Wang, C. Ji, W. Xu, H. Wang, Preparation, physicochemical properties and biocompatibility of PBLG/PLGA/bioglass composite scaffolds, Mater. Sci. Eng. C Mater. Biol. Appl. 71 (2017) 118–124.

[38] Y. Yang, X.Y. Xie, X.G. Mei, Preparation and in vitro evaluation of thienorphine-loaded PLGA nanoparticles, Drug Deliv 23 (3) (2016) 787–793.

[39] X. Zhao, Y. Han, J. Li, B. Cai, H. Gao, W. Feng, S. Li, J. Liu, D. Li, BMP-2 immobilized PLGA/hydroxyapatite fibrous scaffold via polydopamine stimulates osteoblast growth, Mater. Sci. Eng. C Mater. Biol. Appl. 78 (2017) 658–666.

[40] L. Tian, J. Gao, Z. Yang, Z. Zhang, G. Huang, Tamibarotene-loaded PLGA microspheres for intratumoral injection administration: preparation and evaluation, AAPS PharmSciTech 19 (1) (2018) 275–283.

[41] W. Fan, D. Liu, Y. Li, Q. Sun, B. Fan, AgCa-PLGA submicron particles inhibit the growth and colonization of *E. faecalis* and *P. gingivalis* on dentin through infiltration

[42] W. Fan, Y. Li, D. Liu, Q. Sun, M. Duan, B. Fan, PLGA submicron particles containing chlorhexidine, calcium and phosphorus inhibit *Enterococcus faecalis* infection and improve the microhardness of dentin, J Mater Sci Mater 30 (2) (2019) 17.

[43] B.M. Priyadarshini, K. Mitali, T.B. Lu, H.K. Handral, N. Dubey, A.S. Fawzy, PLGA nanoparticles as chlorhexidine-delivery carrier to resin-dentin adhesive interface, Dent. Mater. 33 (7) (2017) 830–846.

[44] T. Kokubo, H. Takadama, How useful is SBF in predicting in vivo bone bioactivity? Biomaterials 27 (15) (2006) 2907–2915.

[45] N. Cohenca, P.C. Romualdo, L.A. da Silva, R.A. da Silva, A.M. de Queiroz, A. De Rossi, P. Nelson-Filho, Tissue response to root canal irrigation systems in dogs' teeth with apical periodontitis, Clin. Oral Investig. 19 (5) (2015) 1147–1156.

[46] A.H. Weerkamp, H.M. Uyen, H.J. Busscher, Effect of zeta potential and surface energy on bacterial adhesion to uncoated and saliva-coated human enamel and dentin, J. Dent. Res. 67 (12) (1988) 1483–1487.

[47] M. Prado, E.J. Silva, T.M. Duque, A.A. Zaia, C.C. Ferraz, J.F. Almeida, Antimicrobial and cytotoxic effects of phosphoric acid solution compared to other root canal irrigants, J. Appl. Oral Sci. 23 (2015) 158–163.

[48] C. Martins, F. Sousa, F. Araujo, B. Sarmento, Functionalizing PLGA and PLGA derivatives for drug delivery and tissue regeneration applications, Adv Healthc Mater 7 (1) (2018) 1701035.

[49] M.M. Meghil, F. Rueggeberg, A. El-Awady, B. Miles, F. Tay, D. Pashley, C.W. Cutler, Novel coating of surgical suture confers antimicrobial activity against *Porphyromonas gingivalis* and *Enterococcus faecalis*, J. Periodontol. 86 (6) (2015) 788–794.

[50] T. Matoba, K. Egashira, Nanoparticle-mediated drug delivery system for cardio-vascular disease, Int. Heart J. 55 (4) (2014) 281–286.

[51] M. Giannelli, F. Chellini, M. Margheri, P. Tonelli, A. Tani, Effect of chlorhexidine digluconate on different cell types: a molecular and ultrastructural investigation, Toxicol. in Vitro 22 (2008) 308–317.

[52] D. Umer, C.K. Yiu, M.F. Burrow, L.N. Niu, F.R. Tay, Effect of a novel quaternary ammonium silane on dentin protease activities, J. Dent. 58 (2017) 19–27.

[53] J.J.M. Damen, J.M. Ten Cate, The effect of silicic acid on calcium phosphate precipitation, J. Dent. Res. 68 (9) (1989) 1355–1359.

[54] L. Han, S. Kodama, T. Okiji, Evaluation of calcium-releasing and apatite-forming abilities of fast-setting calcium silicate-based endodontic materials, Int. Endod. J. 48 (2) (2015) 124–130.

[55] G. Hinata, K. Yoshiba, L. Han, N. Edanami, N. Yoshiba, T. Okiji, Bioactivity and biomineralization ability of calcium silicate-based pulp-capping materials after subcutaneous implantation, Int. Endod. J. 50 (Suppl. 2) (2017) e40–e51.

[56] C. Li, C. Jiang, Y. Deng, T. Li, N. Li, M. Peng, J. Wang, RhBMP-2 loaded 3D-printed mesoporous silica/calcium phosphate cement porous scaffolds with enhanced vascularization and osteogenesis properties, Sci. Rep. 7 (2017) 41331.

[57] Z. Dong, J. Chang, Y. Deng, A. Joiner, Tricalcium silicate induced mineralization for occlusion of dentinal tubules, Aust. Dent. J. 56 (2) (2011) 175–180.

[58] S. Liu, Y. Sun, Y. Fu, D. Chang, C. Fu, G. Wang, Y. Liu, F.R. Tay, Y. Zhou, Bioinspired collagen-apatite nanocomposites for bone regeneration, J Endod 42 (8) (2016) 1226–1232.

[59] P.Z. Tawil, M. Trope, A.E. Curran, D.J. Caplan, A. Kirakozova, D.J. Duggan, F.B. Teixeira, Periapical microsurgery: an in vivo evaluation of endodontic root-end filling materials, J Endod 35 (3) (2009) 357–362.

[60] N. Yamauchi, S. Yamauchi, H. Nagaoka, D. Duggan, S. Zhong, S.M. Lee, F.B. Teixeira, M. Yamauchi, Tissue engineering strategies for immature teeth with apical periodontitis, J Endod 37 (3) (2011) 390–397.

[61] K. Otani, T. Sugaya, M. Tomita, Y. Hasegawa, H. Miyaji, T. Tenkumo, S. Tanaka, Y. Motoki, Y. Takanawa, M. Kawanami, Healing of experimental apical periodontitis after apicoectomy using different sealing materials on the resected root end, Dent. Mater. 30 (4) (2011) 485–492.

[62] I. Chen, B. Karabucak, C. Wang, H.G. Wang, E. Koyama, M.R. Kohli, H.D. Nah, S. Kim, Healing after root-end microsurgery by using mineral trioxide aggregate and a new calcium silicate-based bioceramic material as root-end filling materials in dogs, J Endod 41 (3) (2015) 389–399.

[63] R. Shrivastava, V.K. Rai, A. Kumar, S. Sinha, P. Tripathi, K. Gupta, S. Sabharwal, An in vitro comparison of endodontic medicaments propolis and calcium hydroxide alone and in combination with ciprofloxacin and moxifloxacin against *Enterococcus faecalis*, J. Contemp. Dent. Pract. 16 (5) (2015) 394–399.

[64] S. Taneja, P. Kumar, K. Malhotra, J. Dhillon, Antimicrobial effect of an ox-azolidinone, lantibiotic and calcium hydroxide against Enterococcus faecalis biofilm: an in vitro study, Indian J Dent 6 (4) (2015) 190–194.

[65] W. Fan, Y. Wu, T. Ma, Y. Li, B. Fan, Substantivity of Ag-Ca-Si mesoporous nanoparticles on dentin and its ability to inhibit *Enterococcus faecalis*, J Mater Sci Mater Med 27 (1) (2016) 16.

[66] J.A. Soares, M.R. Leonardo, L.B. Silva, M. Tanomaru Filho, I.Y. Ito, Histomicrobiologic aspects of the root canal system and periapical lesions in dogs' teeth after rotary instrumentation and intracanal dressing with Ca(OH)₂ pastes, J. Appl. Oral Sci. 14 (5) (2006) 355–364.

[67] M. Tanomaru Filho, J.C. Yamashita, M.R. Leonardo, L.B. Silva, J.M.G. Tanomaru, I.Y. Ito, In vivo microbiological evaluation of the effect of biomechanical preparation of root canals using different irrigating solutions, J. Appl. Oral Sci. 14 (2) (2006) 105–110.

[68] A. De Rossi, L.A. Silva, P. Gaton-Hernandez, M.D. Sousa-Neto, P. Nelson-Filho, R.A. Silva, A.M. de Queiroz, Comparison of pulpal responses to pulpotomy and pulp capping with biodentine and mineral trioxide aggregate in dogs, J Endod 40 (9) (2014) 1362–1369.

[69] G.B. Carr, R.S. Schwartz, C. Schaudinn, A. Gorur, J.W. Costerton, Ultrastructural examination of failed molar retreatment with secondary apical periodontitis: an

examination of endodontic biofilms in an endodontic retreatment failure, J Endod 35 (9) (2009) 1303–1309.

[70] C.M. Pucinelli, L. Silva, N. Cohenca, P.C. Romualdo, R. Silva, A. Consolaro, A.M. Queiroz, P.F. Nelson, Apical negative pressure irrigation presents tissue compatibility in immature teeth, J. Appl. Oral Sci. 25 (6) (2017) 612–619.

[71] T. Shibutani, J.N.M. Heersche, Effect of medium pH on osteoclast activity and

osteoclast formation in cultures of dispersed rabbit osteoclasts, J. Bone Miner. Res. 8 (3) (1993) 331–336.

[72] R.A. da Silva, M.R. Leonardo, L.A. da Silva, L.M. de Castro, A.L. Rosa, P.T. de Oliveira, Effects of the association between a calcium hydroxide paste and 0.4% chlorhexidine on the development of the osteogenic phenotype in vitro, J Endod 34 (2008) 1485–1489.